

## A Distributed Snow-Evolution Modeling System (SnowModel)

GLEN E. LISTON

*Cooperative Institute for Research in the Atmosphere, Colorado State University, Fort Collins, Colorado*

KELLY ELDER

*Rocky Mountain Research Station, USDA Forest Service, Fort Collins, Colorado*

(Manuscript received 17 October 2005, in final form 29 March 2006)

### ABSTRACT

SnowModel is a spatially distributed snow-evolution modeling system designed for application in landscapes, climates, and conditions where snow occurs. It is an aggregation of four submodels: MicroMet defines meteorological forcing conditions, EnBal calculates surface energy exchanges, SnowPack simulates snow depth and water-equivalent evolution, and SnowTran-3D accounts for snow redistribution by wind. Since each of these submodels was originally developed and tested for nonforested conditions, details describing modifications made to the submodels for forested areas are provided. SnowModel was created to run on grid increments of 1 to 200 m and temporal increments of 10 min to 1 day. It can also be applied using much larger grid increments, if the inherent loss in high-resolution (subgrid) information is acceptable. Simulated processes include snow accumulation; blowing-snow redistribution and sublimation; forest canopy interception, unloading, and sublimation; snow-density evolution; and snowpack melt. Conceptually, SnowModel includes the first-order physics required to simulate snow evolution within each of the global snow classes (i.e., ice, tundra, taiga, alpine/mountain, prairie, maritime, and ephemeral). The required model inputs are 1) temporally varying fields of precipitation, wind speed and direction, air temperature, and relative humidity obtained from meteorological stations and/or an atmospheric model located within or near the simulation domain; and 2) spatially distributed fields of topography and vegetation type. SnowModel's ability to simulate seasonal snow evolution was compared against observations in both forested and nonforested landscapes. The model closely reproduced observed snow-water-equivalent distribution, time evolution, and interannual variability patterns.

### 1. Introduction

All global snow-covered environments possess spatial distribution and time evolution characteristics. Further, at the most rudimentary level, all snow covers experience the common factors of accumulation and ablation. These basic features are inherent, regardless of where the snow occurs or the characteristics it possesses (e.g., those associated with the global snow-cover classes: ice, tundra, taiga, alpine/mountain, prairie, maritime, and ephemeral; Sturm et al. 1995). For example, an ephemeral snow cover experiences accumulation and melt processes at nearly the same time, while mountain snowpacks normally have a distinct accumu-

lation season followed by a well-defined ablation season. Another example includes snowfall in the centers of the Greenland and Antarctic ice sheets, where they typically experience year-round accumulation.

Accumulation and ablation can have considerable spatial and temporal variability. This variability is controlled by a combination of spatially and temporally variable atmospheric forcing conditions and how those forcings interact with relatively static local topography and vegetation distributions. Collectively, interactions among meteorology, topography, and vegetation produce snow covers that can have considerable spatial variability and can change significantly over time (e.g., Elder et al. 1991; Blöschl 1999; Balk and Elder 2000; Liston and Sturm 2002; Liston et al. 2002; Essery and Pomeroy 2004).

Snow and its temporally evolving spatial distribution are important in a wide range of environments. For example, snow's relatively high albedo reflects much

---

*Corresponding author address:* Dr. Glen E. Liston, Cooperative Institute for Research in the Atmosphere, Colorado State University, Fort Collins, CO 80523-1375.  
E-mail: liston@cira.colostate.edu

more of the incoming solar radiation back to space than snow-free areas of earth, resulting in a considerable influence on air temperatures and atmospheric circulation patterns (Ellis and Leathers 1999; Cohen and Entekhabi 2001). At finer scales, snow cover influences atmospheric and ground temperatures by moderating the conductive, sensible, and latent energy transfers among the atmosphere, snow cover, and ground (Liston 1995; Hinzman et al. 1998; Nelson et al. 1998). Snow's low thermal conductivity insulates the soil from low winter air temperatures, leaving soils much warmer than they would be otherwise, and leading to lower nighttime air temperatures (Taras et al. 2002; Zhang et al. 2003). Snow cover affects soil-moisture conditions, runoff, and active-layer characteristics (Kane et al. 1991; Hinzman et al. 1996; Marsh 1999), and the snow distribution can impact spring snowmelt-runoff timing, magnitude, and spatial variability (Luce et al. 1998). In the Arctic, snow-cover trends have directly impacted growing season length (Groisman et al. 1994; Tucker et al. 2001). Snow distribution indirectly affects stream channel pattern, morphology, and fluvial processes through thermal controls on permafrost and active layer thickness (McNamara et al. 1999), and impacts active-layer enrichment through thermal regulation of active-layer depth and water/nutrient supply (McNamara et al. 1997). And finally, snow distributions play a critical role by acting as a freshwater reservoir that produces snowmelt runoff providing water for agricultural, domestic, industrial, and other uses. This snowmelt is particularly crucial for populations living in midlatitude arid regions such as the southwestern United States. Snow-covered mountainous terrain in the headwaters of these arid regions can contribute 50% to 80% of the annual downstream water supply (Wahl 1992).

At each point in a landscape, the snow evolution can be described by a snow/water mass balance. Given the energies associated with melt and sublimation processes, the mass balance is intimately coupled to the energy balance. Changes in mass and energy balances govern the snow-cover distribution and evolution at each point in space and time, and include precipitation (solid and liquid), snowmelt, snow metamorphism (affecting factors such as density, thermal conductivity, permeability, and albedo), redistribution by wind, static-surface sublimation, blowing-snow sublimation, snow interception in forest canopies, sublimation of canopy-intercepted snow, snowpack ripening (snowpack temperature increasing to 0°C during melt), and snowpack runoff. These processes, and their attendant impacts on snow-cover distribution and evolution, can

be described mathematically and combined to form a snow-evolution modeling system.

This paper describes SnowModel, a spatially distributed snow-evolution model specifically designed to be applicable over a wide range of snow landscapes, climates, and conditions. SnowModel incorporates four submodels: MicroMet defines the meteorological forcing conditions, EnBal calculates the surface energy exchanges, SnowPack simulates snow depth and water-equivalent evolution, and SnowTran-3D accounts for snow redistribution by wind. In what follows, each of the submodels is described. In addition, since each of these submodels was originally developed and tested for nonforested conditions, details describing modifications made to the submodels for forested areas are provided (e.g., forest-radiation and forest-wind interactions, and sublimation from canopy-intercepted snow).

While other distributed snow models exist that simulate the full seasonal snow evolution, most of them do not include blowing-snow redistribution processes (e.g., Tarboton et al. 1995; Marks et al. 1999) [Tarboton et al. (1995) did include an empirical "drift factor"]. An exception to this was provided by Winstral and Marks (2002) when they coupled the Winstral et al. (2002) terrain-based snow redistribution model with the Marks et al. (1999) image-based energy balance snowmelt model (ISNOBAL). SnowModel also includes a blowing-snow submodel (SnowTran-3D) (Liston and Sturm 1998; Liston et al. 2006, manuscript submitted to *J. Glaciol.*) and provides an alternative approach that has been tested over a range of blowing-snow environments (e.g., Colorado (Greene et al. 1999), Antarctica (Liston et al. 2000; Liston and Winther 2005), Idaho (Prasad et al. 2001); Wyoming (Hiemstra et al. 2002), Alaska (Liston and Sturm 2002; Liston et al. 2002), Greenland (Hasholt et al. 2003; Mernild et al. 2006), Svalbard/Norway (Bruland et al. 2004), and the European Alps (U. Strasser 2006, personal communication). Prasad et al. (2001) coupled SnowTran-3D with the Utah energy balance (UEB) model (Tarboton et al. 1995) to simulate seasonal snow evolution. The existence of a blowing and drifting snow component within a distributed snow model allows application in arctic, alpine, and grassland environments: environments that comprise 68% of seasonally snow-covered Northern Hemisphere land (Liston 2004).

## 2. SnowModel description

SnowModel is designed to run on grid increments of 1 to 200 m and temporal increments of 10 min to 1 day. Represented processes include accumulation from snow precipitation; blowing-snow redistribution and

sublimation; interception, unloading, and sublimation within forest canopies; snow-density evolution; and snowpack ripening and melt. SnowModel includes the first-order physics required to simulate snow evolution within each of the global snow classes defined by Sturm et al. (1995) (i.e., ice, tundra, taiga, alpine/mountain, prairie, maritime, and ephemeral). The model can be applied using much larger grid increments, if the inherent loss in high-resolution (subgrid) information is acceptable.

Required SnowModel inputs are 1) temporally varying fields of precipitation, wind speed and direction, air temperature, and relative humidity, obtained from meteorological stations and/or an atmospheric model located within or near the simulation domain; and 2) spatially distributed topography and vegetation type. The number of grid cells and their associated increments in the  $x$  and  $y$  directions within the computational domain are user defined and primarily limited by available computer resources.

#### *a. MicroMet*

MicroMet is a quasi-physically-based, high-resolution (e.g., 1-m to 1-km horizontal grid increment), meteorological distribution model (Liston and Elder 2006). The model was designed specifically to produce high-resolution meteorological forcing distributions required to run spatially distributed terrestrial models over a wide variety of landscapes. It is a data assimilation and interpolation model that utilizes meteorological station datasets, remote sensing observations, and/or gridded atmospheric model or analyses datasets. The model uses known relationships between meteorological variables and the surrounding landscape (primarily topography) to distribute those variables over any given landscape in computationally efficient and physically plausible ways. MicroMet performs two kinds of adjustments to the meteorological data: 1) all available data, at a given time, are spatially interpolated over the domain, and 2) physical submodels are applied to each MicroMet variable to improve realism at a given point in space and time. At each time step, MicroMet generates distributions of 1) air temperature, 2) relative humidity, 3) wind speed, 4) wind direction, 5) incoming solar radiation, 6) incoming longwave radiation, 7) surface pressure, and 8) precipitation. These distributed data are the fundamental atmospheric forcing variables required to run most terrestrial models.

Early versions of MicroMet have been used to distribute observed and modeled meteorological variables over complex terrain in Colorado, Wyoming, Idaho, Arctic Alaska, Svalbard, central Norway, Greenland, and Antarctica as part of a wide variety of terrestrial

modeling studies (e.g., Liston and Sturm 1998, 2002; Greene et al. 1999; Liston et al. 1999b, 2002; Hiemstra et al. 2002; Prasad et al. 2001; Hasholt et al. 2003; Bruland et al. 2004; Liston and Winther 2005).

MicroMet includes a preprocessor that analyzes meteorological data and identifies and corrects potential deficiencies. Since providing temporally and spatially continuous atmospheric forcing data for terrestrial models is a core objective of MicroMet, the preprocessor also fills in any missing data segments with realistic values. Additional details are provided by Liston and Elder (2006).

MicroMet does station (horizontal) interpolations using a Barnes objective analysis scheme (Barnes 1964, 1973; Koch et al. 1983). Objective analysis is the process of interpolating data from irregularly spaced stations to a regular grid. The Barnes scheme applies a Gaussian distance-dependent weighting function, where the weight that a station contributes to the overall value of the grid point decreases with increasing distance from the point. In MicroMet, the interpolation weights are objectively determined as a function of the data spacing and distribution.

The following descriptions summarize MicroMet procedures implemented to adjust and distribute each meteorological variable. The model assumes that, at a minimum, screen-height air temperature, relative humidity, wind speed and direction, and precipitation, are available at each time of interest.

- 1) *Air temperature*: Historically, simple interpolation routines have been used to spatially distribute point air temperature data. While these methods work in flat terrain, they generally misrepresent temperature distributions in areas having significant topographic variability. Recent studies have tried to improve the simulated temperature distributions by taking advantage of the strong temperature–elevation relationships that are known to exist (Dodson and Marks 1997). In MicroMet, station air temperatures are adjusted to a common level, using either a lapse rate given by Kunkel (1989) that varies depending on the month of the year, or calculated based on adjacent station data. The reference-level station temperatures are then interpolated to the model grid using the Barnes objective analysis scheme. The available gridded topography data and Kunkel (1989) (or observed) lapse rate are then used to adjust the reference-level gridded temperatures to the elevations provided by the topography dataset.
- 2) *Relative humidity*: Since relative humidity is a nonlinear function of elevation, the relatively linear

dewpoint temperature is used for the elevation adjustments. First, MicroMet converts the station relative humidity to dewpoint temperature. Then the dewpoint temperatures at the stations are adjusted to a common reference level using a monthly varying dewpoint temperature lapse rate defined by Kunkel (1989) (or the observations). The reference-level station dewpoint temperatures are then interpolated to the model grid using the Barnes objective analysis scheme. The dewpoint lapse rate is used to take the reference-level gridded values to the actual topographic elevations using the dewpoint temperature lapse rate. These gridded dewpoint temperature values are then converted to relative humidity.

- 3) *Wind speed* and 4) *Wind direction*: Station wind speed and direction are converted to zonal ( $u$ ) and meridional ( $v$ ) components that are then independently interpolated to the model grid using the Barnes objective analysis scheme. The resulting wind speed and direction values are modified using a simple, topographically driven wind model following Liston and Elder (2006) that adjusts the speeds according to topographic slope and curvature relationships. The wind directions are modified by a topographic diverting factor defined by Ryan (1977).
- 5) *Solar radiation*: The incoming solar radiation model includes the influence of time, cloud cover, direct and diffuse solar radiation, and topographic slope and aspect, on incoming solar radiation (Liston et al. 1999b). Cloud cover is accounted for by taking the surface gridded temperature and dewpoint fields (described above), and the associated lapse rates, to calculate temperature and dewpoint at 700 mb. These temperature and dewpoint surfaces are then used to calculate the 700-mb relative humidity. Following Walcek (1994), and assuming a minimum averaging dimension, this 700-mb relative humidity distribution is used to define the cloud fraction. MicroMet can also assimilate incoming solar radiation observations into these calculations.
- 6) *Longwave radiation*: Incoming longwave radiation is calculated while taking into account cloud cover and elevation-related variations following Iziomon et al. (2003). This modeling approach is particularly valid for domains covering a wide range of elevations. Incoming longwave radiation observations can also be assimilated.
- 7) *Surface pressure*: In the absence of surface pressure observations, a time-independent atmospheric pressure distribution is provided following Wallace and Hobbs (1977).
- 8) *Precipitation*: To distribute precipitation over the domain, observed precipitation values are first in-

terpolated to the model grid using the Barnes objective analysis scheme. To generate a topographic reference surface, the station elevations are also interpolated to the model grid. Since the precipitation adjustment function is a nonlinear function of elevation difference (Liston and Elder 2006), the interpolated station elevations are used as the topographic reference surface (instead of sea level). The modeled liquid-water precipitation rate is set equal to the product of the interpolated station precipitation and a monthly varying empirical topographic adjustment factor (Thornton et al. 1997). This approach results in a nonlinear precipitation increase (decrease) with increasing (decreasing) elevation from the topographic reference surface.

#### b. *EnBal*

This model performs standard surface energy balance calculations (Liston 1995; Liston et al. 1999b). It simulates surface (skin) temperatures, and energy and moisture fluxes in response to observed and/or modeled near-surface atmospheric conditions provided by MicroMet. Surface latent and sensible heat flux, and snowmelt calculations are made using a surface energy balance model of the form

$$(1 - \alpha)Q_{si} + Q_{li} + Q_{le} + Q_h + Q_e + Q_c = Q_m, \quad (1)$$

where  $Q_{si}$  is the solar radiation reaching earth's surface,  $Q_{li}$  is the incoming longwave radiation,  $Q_{le}$  is the emitted longwave radiation,  $Q_h$  is the turbulent exchange of sensible heat,  $Q_e$  is the turbulent exchange of latent heat,  $Q_c$  is the conductive energy transport,  $Q_m$  is the energy flux available for melt, and  $\alpha$  is the surface albedo. For snow and ice surfaces, SnowModel defines different albedos for the snow below forest canopies, the snow in forest-free areas, and for glacier ice. Details of each term in Eq. (1), and the model solution, can be found in Liston (1995), Liston and Hall (1995), and Liston et al. (1999b). In this model, each term in the surface energy balance is computed by applying equations that have been cast in a form that leaves the surface temperature as the only unknown. The melt energy is defined to be zero, and Eq. (1) is solved iteratively for the surface temperature. In the presence of snow, surface temperatures greater than 0°C indicate that energy is available for melting. This energy is computed by fixing the surface temperature at 0°C and solving Eq. (1) for  $Q_m$ .

#### c. *SnowPack*

SnowPack is a simple, single-layer, snowpack evolution model (Liston and Hall 1995) that defines snow-



TABLE 1. Predefined SnowModel vegetation types and associated snow-holding depths. In the model the canopy heights are assumed to equal the snow-holding depths. Also included are the maximum (summer) and minimum (winter) LAI\* values for the forest types.

	Class	Description	Example	Snow-holding depth (m)	LAI* max/min
1	Forest	Coniferous forest	Spruce-fir/taiga/lodgepole	15.00	2.5/2.5
2	Forest	Deciduous forest	Aspen forest	12.00	2.5/0.5
3	Forest	Mixed forest	Aspen/spruce-fir/low taiga	14.00	2.5/1.5
4	Forest	Scattered short-conifer	Pinyon-juniper	8.00	1.5/1.5
5	Forest	Clearcut conifer	Stumps and regenerating	4.00	1.0/1.0
6	Shrub	Mesic upland shrub	Deeper soils, less rocky	0.50	—
7	Shrub	Xeric upland shrub	Rocky, windblown soils	0.25	—
8	Shrub	Playa shrubland	Greasewood, saltbush	1.00	—
9	Shrub	Shrub wetland/riparian	Willow along streams	1.75	—
10	Shrub	Erect shrub tundra	Arctic shrubland	0.65	—
11	Shrub	Low shrub tundra	Low to medium arctic shrubs	0.30	—
12	Grass	Grassland rangeland	Graminoids and forbs	0.15	—
13	Grass	Subalpine meadow	Meadows below treeline	0.25	—
14	Grass	Tundra (nontussock)	Alpine, high arctic	0.15	—
15	Grass	Tundra (tussock)	Graminoids and dwarf shrubs	0.20	—
16	Grass	Prostrate shrub tundra	Graminoid dominated	0.10	—
17	Grass	Arctic gram, wetland	Grassy wetlands, wet tundra	0.20	—
18	Bare	Bare	—	0.01	—
19	Water	Water/possibly frozen	—	0.01	—
20	Water	Permanent snow/glacier	—	0.01	—
21	Human	Residential/urban	—	0.01	—
22	Human	Tall crops	Corn stubble	0.40	—
23	Human	Short crops	Wheat stubble	0.25	—

pack changes in response to the precipitation and melt fluxes defined by MicroMet. This is a different model than SNOWPACK described by Bartelt and Lehning (2002). SnowPack's formulation closely follows Anderson (1976) to define compaction-based snow-density evolution. In SnowPack, the density changes with time in response to snow temperature and weight of overlying snow. A second density-modifying process results from snow melting. The melted snow decreases snow depth and the associated meltwater is redistributed through the snowpack until a maximum snow density is reached. Any additional meltwater is assumed to reach the ground at the base of the snowpack. The density of new snow from additional accumulation is defined following Anderson (1976) (cf. Liston and Hall 1995). Static-surface (nonblowing snow) sublimation calculated in EnBal is used to adjust the snowpack depth; blowing-snow sublimation is calculated in SnowTran-3D.

#### d. SnowTran-3D

SnowTran-3D is a three-dimensional model that simulates snow-depth evolution resulting from wind-blown snow (Liston and Sturm 1998; Liston et al. 2006, manuscript submitted to *J. Glaciol.*). The model was originally developed and tested in an Alaska arctic-tundra landscape (Liston and Sturm 1998, 2002), but has also been applied in other treeless alpine, arctic,

and Antarctic areas of the world characterized by sufficiently strong winds, below-freezing temperatures, and solid precipitation (Greene et al. 1999; Liston et al. 2000; Prasad et al. 2001; Hiemstra et al. 2002; Liston and Sturm 2002; Hasholt et al. 2003; Bruland et al. 2004). SnowTran-3D's primary components are 1) the wind-flow forcing field; 2) the wind shear stress on the surface; 3) the transport of snow by saltation; 4) the transport of snow by turbulent suspension; 5) the sublimation of saltating and suspended snow; and 6) the accumulation and erosion of snow at the snow surface. The required model inputs are 1) spatially distributed, temporally varying fields of precipitation, wind speed and direction, air temperature, and humidity, obtained from MicroMet; and 2) spatially distributed fields of topography and vegetation type.

SnowModel includes 23 predefined and 7 user-defined vegetation types (Table 1). Within the model, each grid cell is assigned a single vegetation type, and each vegetation type is assigned a canopy height that defines the vegetation snow-holding depth (Table 1). The simulated snow depth must exceed the vegetation snow-holding depth before snow becomes available for wind transport (i.e., snow captured within the vegetation canopy by either precipitation or blowing-snow deposition cannot be removed by wind). As a result of these important snow-vegetation interactions (Mc-

Fadden et al. 2001; Sturm et al. 2001; Liston et al. 2002; Essery and Pomeroy 2004; Strack et al. 2003), SnowTran-3D simulates the snow-depth evolution, then uses the snow density to convert to the more hydrologically relevant snow water equivalent (SWE).

The foundation of SnowTran-3D is a mass-balance equation that describes the temporal variation of snow depth at each point within the simulation domain (Liston and Sturm 1998). Deposition and erosion, which lead to changes in snow depth at these points, are the result of 1) changes in horizontal mass-transport rates of saltation,  $Q_{\text{salt}}$  ( $\text{kg m}^{-1} \text{s}^{-1}$ ), 2) changes in horizontal mass-transport rates of turbulent-suspended snow,  $Q_{\text{turb}}$  ( $\text{kg m}^{-1} \text{s}^{-1}$ ), 3) sublimation of transported snow particles,  $Q_v$  ( $\text{kg m}^{-2} \text{s}^{-1}$ ), and 4) the water-equivalent precipitation rate,  $P$  ( $\text{m s}^{-1}$ ). Combined, the time rate of change of snow depth,  $\zeta$  (m), is

$$\frac{d(\rho_s \zeta)}{dt} = \rho_w P - \left( \frac{dQ_{\text{salt}}}{dx} + \frac{dQ_{\text{turb}}}{dx} + \frac{dQ_{\text{salt}}}{dy} + \frac{dQ_{\text{turb}}}{dy} \right) + Q_v, \quad (2)$$

where  $t$  (s) is time;  $x$  (m) and  $y$  (m) are the horizontal coordinates in the west-east and south-north directions, respectively; and  $\rho_s$  and  $\rho_w$  ( $\text{kg m}^{-3}$ ) are the snow and water density, respectively. At each time step, Eq. (1) is solved for each individual grid cell within the domain, and is coupled to the neighboring cells through the spatial derivatives ( $d/dx$ ,  $d/dy$ ).

### 3. SnowModel modifications for forests

The submodels that make up SnowModel were all originally developed for arctic and alpine landscapes that lacked forests. What follows is a summary of the added SnowModel components that allow it to simulate snow evolution in forested environments.

#### a. Sublimation of canopy-intercepted snow

The sublimation of snow held within the forest canopy,  $Q_{\text{cs}}$  ( $\text{kg m}^{-2}$ ), is represented by the combined influences of the sublimation-loss rate coefficient for an ice sphere,  $\Psi_s$  ( $\text{s}^{-1}$ ), the intercepted canopy load,  $I$  ( $\text{kg m}^{-2}$ ), and a nondimensional canopy exposure coefficient,  $C_e$ , that accounts for the fact that the exposed snow surface area is less than the surface area of the individual grains comprising the intercepted snow. Thus,

$$Q_{\text{cs}} = C_e I \Psi_s dt, \quad (3)$$

where  $dt$  (s) is the time increment.

The canopy-intercepted load,  $I$ , at time,  $t$ , is (Pomeroy et al. 1998b)

$$I = I^{t-1} + 0.7(I_{\text{max}} - I^{t-1})[1 - \exp(-P/I_{\text{max}})], \quad (4)$$

where  $t - 1$  indicates the previous time step, and  $P$  ( $\text{kg m}^{-2}$ ) is the snow precipitation for the current time step. Any precipitation not intercepted by the canopy is added to the snow on the ground. The maximum interception storage,  $I_{\text{max}}$  ( $\text{kg m}^{-2}$ ), is (Hedstrom and Pomeroy 1998)

$$I_{\text{max}} = 4.4 \text{LAI}^*, \quad (5)$$

where  $\text{LAI}^*$  is the effective (includes stems, leaves, and branches; Chen et al. 1997) leaf area index ( $\text{m}^2 \text{m}^{-2}$ ). SnowModel includes five forest vegetation types (Table 1). For each of these, a maximum (summer) and minimum (winter) seasonal  $\text{LAI}^*$  value is defined (Table 1) and used to calculate  $\text{LAI}^*$  during each day of the model simulation following Liston and Pielke (2001).

The canopy exposure coefficient,  $C_e$ , is defined following Pomeroy and Schmidt (1993),

$$C_e = k_c \left( \frac{I^t}{I_{\text{max}}} \right)^{-0.4}, \quad (6)$$

where  $k_c$  is a dimensionless coefficient, equal to 0.010, related to the shape of the intercepted snow deposits (see our analysis below).

The sublimation-loss rate coefficient for an ice sphere,  $\Psi_s$  ( $\text{s}^{-1}$ ), is given by

$$\Psi_s = \frac{dm/dt}{m}, \quad (7)$$

where the particle mass,  $m$  (kg), is

$$m = \frac{4}{3} \pi \rho_i r^3, \quad (8)$$

with  $r$  (m) being the radius of a spherical ice particle (assumed to be  $500 \mu\text{m}$ ), and  $\rho_i$  ( $\text{kg m}^{-3}$ ) is ice density. The rate of mass loss from an ice sphere is described by the combined influences of humidity gradients between the particle and the atmosphere, intercepted solar radiation, particle size, and advective (ventilation) influences, and is given by (Thorpe and Mason 1966; Schmidt 1972)

$$\frac{dm}{dt} = \frac{2\pi r \left( \frac{\text{RH}}{100} - 1 \right) - S_p \Omega}{h_s \Omega + \frac{1}{D \rho_v \text{Sh}}}, \quad (9)$$

where  $\text{RH}$  (%) is the relative humidity of the air provided by MicroMet, and  $h_s$  ( $2.838 \times 10^6 \text{ J kg}^{-1}$ ) is the latent heat of sublimation.  $\Omega$  is given by

$$\Omega = \frac{1}{\lambda_t T_a \text{Nu}} \left( \frac{h_s M}{RT_a} - 1 \right), \quad (10)$$

where  $M$  ( $18.01 \text{ kg kmole}^{-1}$ ) is the molecular weight of water,  $R$  ( $8313 \text{ J kmole}^{-1} \text{ K}^{-1}$ ) is the universal gas constant,  $T_a$  (K) is the air temperature provided by MicroMet, and  $\lambda_t$  ( $0.024 \text{ J m}^{-1} \text{ s}^{-1} \text{ K}^{-1}$ ) is the thermal conductivity of the atmosphere. Both the air temperature and the relative humidity are assumed to be constant with height through the canopy. The diffusivity of water vapor in the atmosphere,  $D$  ( $\text{m}^2 \text{ s}^{-1}$ ), is given by (Thorpe and Mason 1966)

$$D = 2.06 \times 10^{-5} (T_a/273)^{1.75}. \quad (11)$$

The saturation density of water vapor,  $\rho_v$  ( $\text{kg m}^{-3}$ ), is (Fleagle and Businger 1980)

$$\rho_v = 0.622 \frac{e_s}{R_d T_a}, \quad (12)$$

where  $R_d$  ( $287 \text{ J deg}^{-1} \text{ kg}^{-1}$ ) is the gas constant for dry air. The saturation vapor pressure over ice,  $e_s$  (Pa), is approximated by (Buck 1981)

$$e_s = 611.15 \exp \left[ \frac{22.452 (T_a - 273.16)}{T_a - 0.61} \right]. \quad (13)$$

The Nusselt (Nu) and Sherwood (Sh) numbers are related to the particle Reynolds number (Re) (Lee 1975):

$$\text{Nu} = \text{Sh} = 1.79 + 0.606 \text{Re}^{0.5}, \quad 0.7 < \text{Re} < 10, \quad (14)$$

with

$$\text{Re} = \frac{2ru_c}{\nu}, \quad (15)$$

where  $\nu$  ( $1.3 \times 10^{-5} \text{ m}^2 \text{ s}^{-1}$ ) is the kinematic viscosity of air, and  $u_c$  ( $\text{m s}^{-1}$ ) is the ventilation velocity, set equal to the wind speed within the canopy.

The canopy wind speed is given by (Cionco 1978)

$$u_c = u \exp[-a(1 - z/h)], \quad (16)$$

where  $u$  ( $\text{m s}^{-1}$ ) is the wind speed above the canopy top,  $h$  (m) is the canopy height, and  $z$  (m) is the canopy wind speed reference level (assumed to be  $0.6h$ ; Essery et al. 2003). The canopy flow index,  $a$  is defined to be

$$a = \beta \text{LAI}^*, \quad (17)$$

where  $\beta = 0.9$  is a scaling factor that adjusts leaf-area-index values to be compatible with the canopy flow indices defined by Cionco (1978).

The solar radiation absorbed by the snow particle,  $S_p$  (W), is

$$S_p = \pi r^2 (1 - \alpha_p) S_i, \quad (18)$$

where  $\alpha_p$  is the snow particle albedo (assumed to be equal to the simulated snow albedo), and  $S_i$  ( $\text{W m}^{-2}$ ) is

the incoming solar radiation at earth's surface. The calculation of  $S_i$  is described in Liston and Elder (2006).

In addition to mass lost by sublimation, intercepted snow is unloaded when canopy air temperatures are above freezing. SnowModel defines a melt-unloading rate,  $L_m$  ( $\text{kg m}^{-2}$ ), based on a temperature index method, that transfers canopy snow to the ground store where it can be melted (the snow does not melt while held by the canopy). An unloading rate of  $5 \text{ kg m}^{-2} \text{ day}^{-1} \text{ K}^{-1}$  is assumed, which leads to the following equation for temperature conditions above freezing:

$$L_m = 5.8 \times 10^{-5} (T_a - 273.16) dt. \quad (19)$$

Our field observations indicate that wind can also have an important influence on unloading canopy-intercepted snow. Unfortunately, it is a complex process that depends on canopy structure and spacing, branch and trunk flexibility, snow temperature and precipitation history, and wind speed and direction. Because of this complexity, existing snow-canopy interception models typically do not include snow unloading by wind. Implementation of a submodel accounting for these processes awaits a field study defining the model requirements.

Model-simulated sublimation of snow held within evergreen forest canopies was compared against Montesi et al.'s (2004) observations from a continental-climate site located within the U.S. Department of Agriculture (USDA) Fraser Experimental Forest ( $39^\circ 53' \text{N}$ ,  $105^\circ 54' \text{W}$ ) near Fraser, Colorado. In their study, they cut, suspended, and continually weighed a 2.7-m-tall subalpine fir tree (*Abies lasiocarpa*) at each of two sites (2920 and 3230 m), from 1 January to 1 May 2001 to estimate sublimation from a fir canopy. Their observational analyses, and our associated model analyses, examined 21 storm-free sublimation periods ranging in duration from 9 to 53 h, for a total of 620 h.

Our simulations solved Eq. (3) for  $Q_{cs}$ , while driving the model with hourly, observed within-canopy air temperature, relative humidity, and wind speed, for both the lower and upper observation sites. Dividing the observed mass by the live tree cross-sectional areas defined the canopy-intercepted load,  $I$ , at each time step. The observed and modeled sublimation rates were converted to units of  $\text{g h}^{-1} \text{ m}^{-2}$  for plotting purposes. For our observation and model comparison, we found a value of  $k_c = 0.010$  provided a best fit to all the observations (620 h, live trees, for both lower and upper sites). This result is similar to the 0.011 value calculated by Pomeroy et al. (1998b) for Canadian boreal forests. Figure 1 shows two diurnal cycles and general agreement among the observed and simulated sublimation

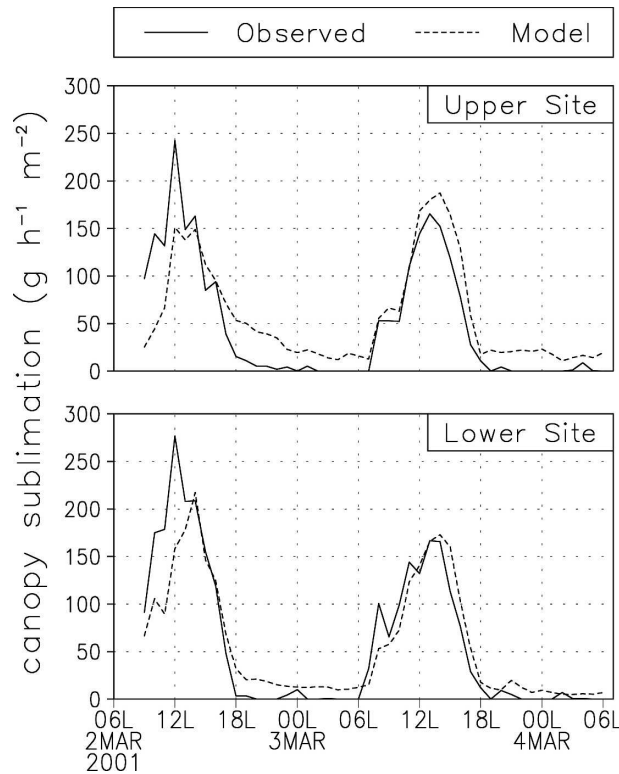


FIG. 1. Observed and modeled evergreen forest snow-in-canopy sublimation rate per unit area for sublimation period 13 as defined by Montesi et al. (2004).

rates for sublimation period 13 defined and analyzed by Montesi et al. (2004). Figure 2a presents a comparison of all the observed and modeled hourly sublimation data, for both the upper and lower tree sites. The total sublimation during each storm-free period was summed as the winter progressed (Fig. 2b). Because of this summing of the Fig. 2a hourly data, overprediction errors have canceled with the underprediction errors, ultimately leading to a modeled mass balance that was comparable to the observed balance over the sublimation season. In addition, by defining the best-fit parameter  $k_c$ , as we have described, the model was forced to fit the observations by the end of the sublimation season. While a single value was defined for this parameter, in Fig. 2b the upper and lower tree data were summed individually. The sublimation magnitudes plotted in Fig. 2b do not match those reported by Montesi et al. (2004) because we did not adjust for intermittent unloading and snowfall events (only a small fraction of the canopy mass balance).

#### b. Radiation adjustments for evergreen forest canopies

Top-of-canopy incoming solar radiation,  $Q_{si}$  ( $W m^{-2}$ ), is modified according to the Beer–Lambert law

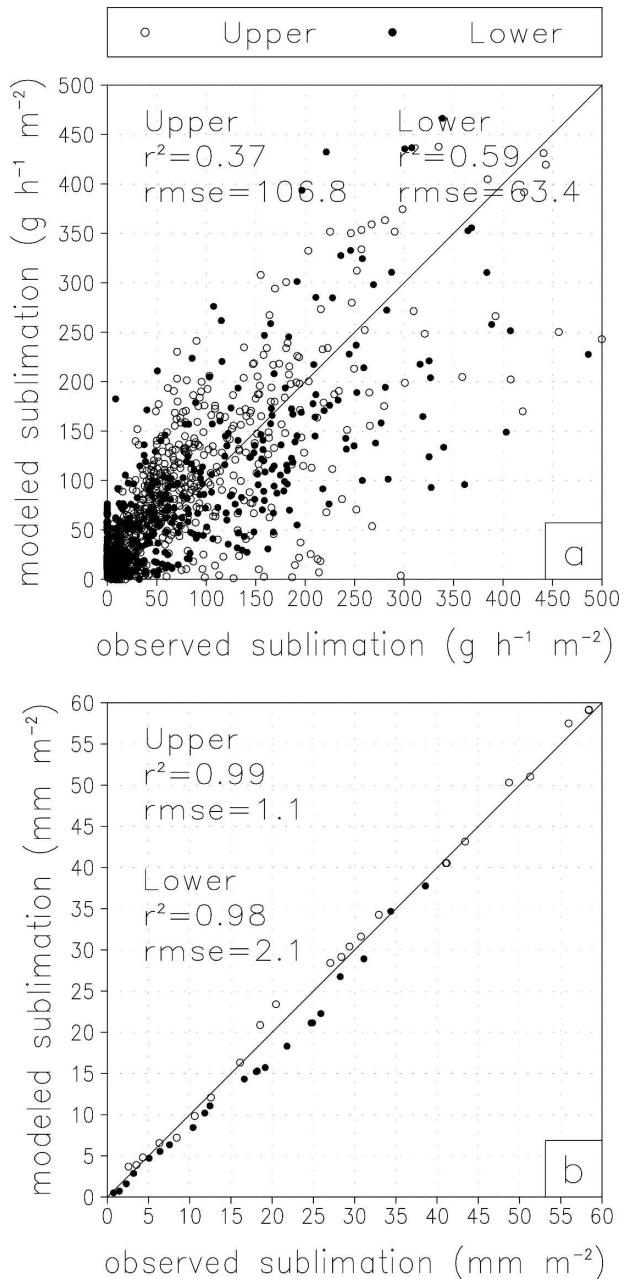


FIG. 2. (a) Observed and modeled hourly sublimation losses for both upper and lower tree sites ( $n = 620$ ). (b) Total sublimation during each storm-free period for upper and lower tree sites, summed as the winter progressed, for each of the 21 sublimation periods defined by Montesi et al. (2004). During this summing, over- and underprediction errors have canceled. In addition, the interception parameter,  $k_c$ , requires the total modeled sublimation to equal the observed. Included are the square of the linear correlation coefficient,  $r^2$ , the root-mean-square error (rmse) values, and the 1:1 line.

following Hellström (2000). The resulting solar radiation reaching the snow surface underneath the canopy,  $Q_{sif}$  ( $W m^{-2}$ ), is

$$Q_{sif} = \tau_v Q_{si}, \quad (20)$$



where the fraction of incoming solar radiation transmitted through the canopy,  $\tau_v$ , is

$$\tau_v = \exp(-k \text{LAI}^*), \quad (21)$$

where  $k$  is a vegetation-dependent extinction coefficient (see discussion below). This formulation includes the multidimensional character of solar radiation interactions with the canopy, including variations in solar zenith angle (Hellström 2000). For conditions where canopy gaps allow incoming solar radiation to reach the ground without canopy modification, SnowModel defines the grid-cell average fraction of incoming solar radiation reaching the ground to be

$$\tau_v = \tau_v(1 - G) + G, \quad (22)$$

where  $\tau_v$  on the right-hand side of Eq. (22) is defined by Eq. (21), and  $G$  (0–1) is the canopy gap fraction.

Above and below canopy radiation data are available from adjacent forested ( $\text{LAI}^* = 2.3$ ) and clear-cut ( $\text{LAI}^* = 0.4$ ) sites of the USDA Fraser Experimental Forest at an elevation of 2800 m (Troendle and Reuss 1997). The forested site is comprised of Englemann spruce (*Picea engelmannii*), subalpine fir (*Abies lasiocarpa*), lodgepole pine (*Pinus contorta* var. *latifolia*), and aspen (*Populus tremuloides*). Using two years (1 October 2001 through 31 August 2003) of hourly incoming solar radiation data from these areas,  $k = 0.71$  produced a modeled best fit to the entire observation period (Fig. 3a). In this analysis, the time periods (mid-winter) with shade produced by surrounding topography have been removed. Figure 3a shows a model underprediction during summer and overprediction during spring and fall. This is possibly related to a relationship between solar zenith angle and canopy structure and could be accounted for by implementing a zenith angle dependence on  $k$  in Eq. (21).

To highlight the difficulty in simulating subcanopy radiation where the true canopy density varies spatially (and the corresponding model grid cell has assumed a uniform canopy), a subset of the Fig. 3a analysis period is shown in Fig. 3b. While the model captures the general observed trends, such a simple formulation is unable to account for radiation peaks that occur when the sun shines through open areas in the trees, and for local variations in cloudiness. This formulation and the associated coefficient value are consistent with the results of Sicart et al. (2004), who found  $\text{LAI}^*$ -dependent  $k$  values ranging from 0.75 for a Colorado forest and 1.0 for Wolf Creek Research Basin, Yukon Territory, Canada. Figure 4 displays the variation of subcanopy incoming solar radiation with variations in  $\text{LAI}^*$ .

The incoming longwave radiation reaching the snow

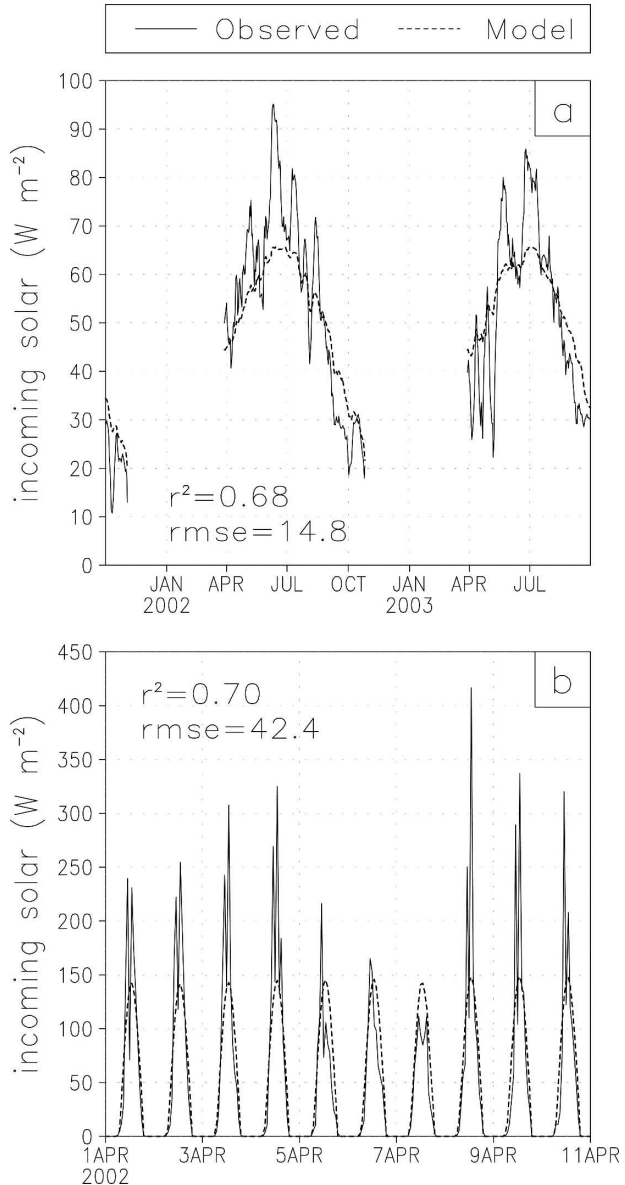


FIG. 3. (a) Time evolution of daily average observed and modeled incoming solar radiation below the evergreen forest canopy ( $\text{LAI}^* = 2.3$ ), for the period 1 Oct 2002–31 Sep 2003. The missing data periods correspond to times when the incoming solar radiation is modified by surrounding topography. (b) A subset of the 2-yr, hourly observation and simulation datasets, showing the model's inability to account for observed radiation spikes resulting from gaps in the forest canopy.

under the canopy,  $Q_{\text{lif}}$  ( $\text{W m}^{-2}$ ), is assumed to equal the fractionally weighted sum of the top-of-canopy incoming longwave radiation,  $Q_{\text{li}}$  ( $\text{W m}^{-2}$ ), coming through gaps in the forest, and the longwave radiation emitted from the forest canopy,

$$Q_{\text{lif}} = (1 - F_c)Q_{\text{li}} + F_c\sigma T_c^4, \quad (23)$$

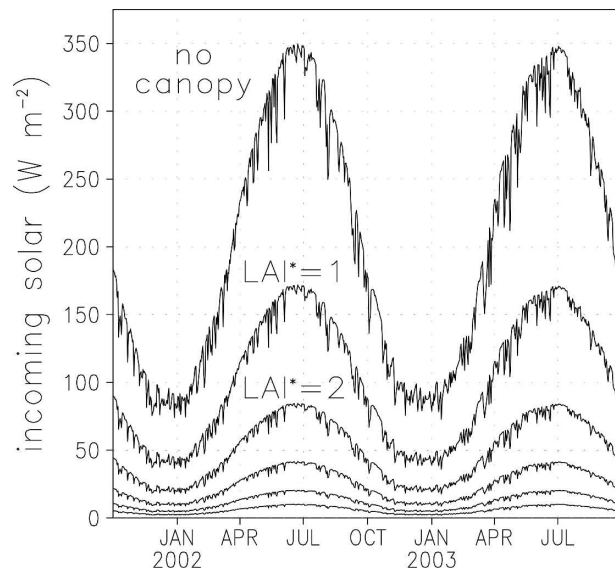


FIG. 4. Variation of model-simulated subcanopy incoming solar radiation with changes in  $\text{LAI}^*$  (for  $\text{LAI}^* = 1, 2, 3, 4$ , and  $5$ ). Plotted are daily average data, 1 Oct 2002–31 Sep 2003. The small radiation variations are the result of MicroMet-simulated cloud cover.

where  $\sigma$  is the Stefan–Boltzmann constant, the canopy temperature,  $T_c$  (K), is assumed in the model to equal the canopy-modified air temperature,  $T_a$ , as defined by MicroMet, and the canopy emissivity is assumed to equal unity (Sicart et al. 2004), and  $F_c$  is the canopy fraction,

$$F_c = a + b \ln(\text{LAI}^*), \quad (24)$$

where  $a = 0.55$  and  $b = 0.29$  are constants (Pomeroy et al. 2002).

The subcanopy longwave radiation model was compared against observations provided by the National Aeronautics and Space Administration (NASA) Cold Land Processes Experiment (CLPX) Local Scale Observation Site (LSOS) meteorological and radiation observing stations (Hardy et al. 2004a) located within the USDA Fraser Experimental Forest. The site consisted of a uniform (managed) lodgepole pine (*Pinus contorta* var. *latifolia*) canopy, with a predicted  $\text{LAI}^*$  of 1.8 (Hardy et al. 2004b). Hourly data from the CLPX 2003 intensive observing periods (19–24 February and 24–30 March 2003) were used for the model comparison (Fig. 5). The simulated incoming subcanopy longwave radiation closely follows the diurnal variations, with a tendency to overestimate the minimum values during the two simulated periods. Simulated above-canopy longwave radiation data were compared against observations in Liston and Elder (2006). Figure 6 shows the

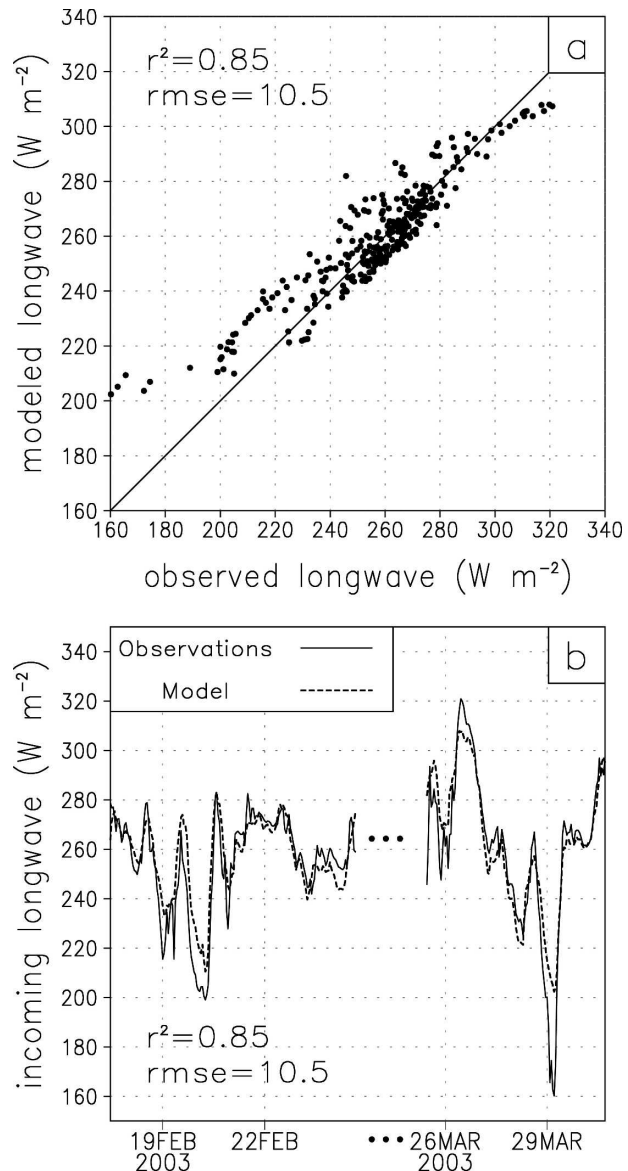


FIG. 5. (a) Hourly average values of observed and modeled incoming longwave radiation below the evergreen forest canopy ( $\text{LAI}^*$  of 1.8), 19–24 Feb and 24–30 Mar 2003, and the 1:1 line. (b) The same data plotted in time series format.

modeled subcanopy incoming longwave radiation sensitivity to  $\text{LAI}^*$ .

#### 4. Example simulations

We have tested the non-forest-related individual SnowModel components as part of other studies and publications (see references cited herein), and have compared the canopy-intercepted-snow sublimation and the forest canopy modifications to incoming solar and longwave radiation against observations as de-

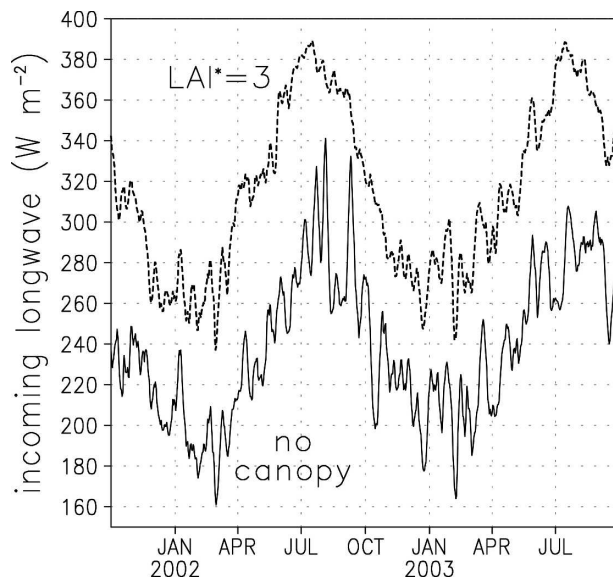


FIG. 6. Variation of model-simulated subcanopy incoming longwave radiation with  $LAI^*$  (for no canopy and  $LAI^* = 3$ ; other  $LAI^*$  values were not plotted to improve visibility). Plotted are daily average data, 1 Oct 2002–31 Sep 2003.

scribed above. In what follows, we analyze SnowModel simulations that use all components of the snow-evolution modeling system (MicroMet, EnBal, SnowPack, and SnowTran-3D).

#### Example SnowModel simulations

To test SnowModel's ability to simulate seasonal snow evolution in forested and nonforested areas, we ran the model over the adjacent forested and clear-cut sites in the Fraser Experimental Forest where we performed our incoming solar radiation analysis (see Fig. 3 discussion). Figure 7 compares the model SWE for the clear-cut and forested areas, and observed SWE collected periodically from snow pits throughout accumulation and melt periods. The model simulations were driven by data from two different meteorological stations located in the clear-cut and forested areas; they span 1 October 2004 through 21 June 2005; and used a 1-h time step. In this area the most notable differences between the forested and nonforested snow-cover observations are the following: the forest typically has less snow at the end of the accumulation period (because of canopy interception losses), and during daytime, forest snow melts slower because less incoming solar radiation reaches the snow surface and the lower wind speeds lead to less sensible heat flux. In addition, in the clearing, longwave radiational cooling at the surface can produce refreezing at night, leading to higher nighttime melting in the forest.

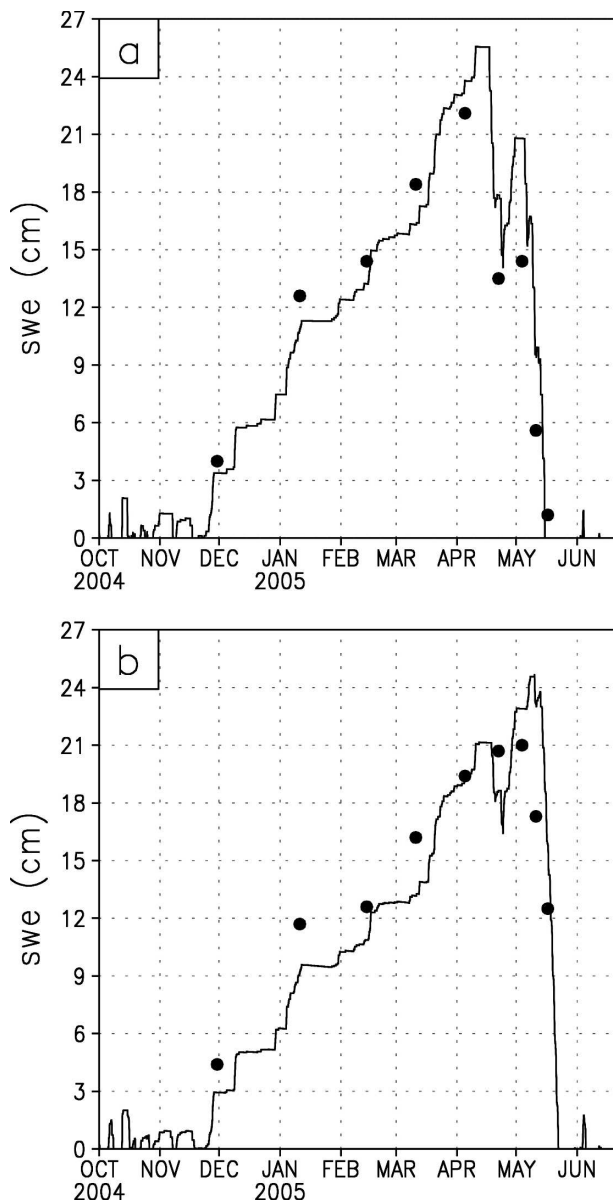


FIG. 7. Modeled (1 Oct 2004–21 Jun 2005) SWE (lines) for the (a) clear-cut and (b) forested sites. Also plotted is the SWE collected from snow pits throughout the accumulation and melt periods (points).

The model captured these features. Figure 8 shows the modeled snow depth evolution for the forested and clear-cut sites, and the observed depth evolution obtained from acoustic depth sensors. Modeled snow density increases more than coincident observed values after a precipitation event, particularly in the forest, sometimes leading to lower simulated snow depths than observed (e.g., during February and March). In general, the model provides a reasonable representation of both the snow depth and SWE time series. These simulations

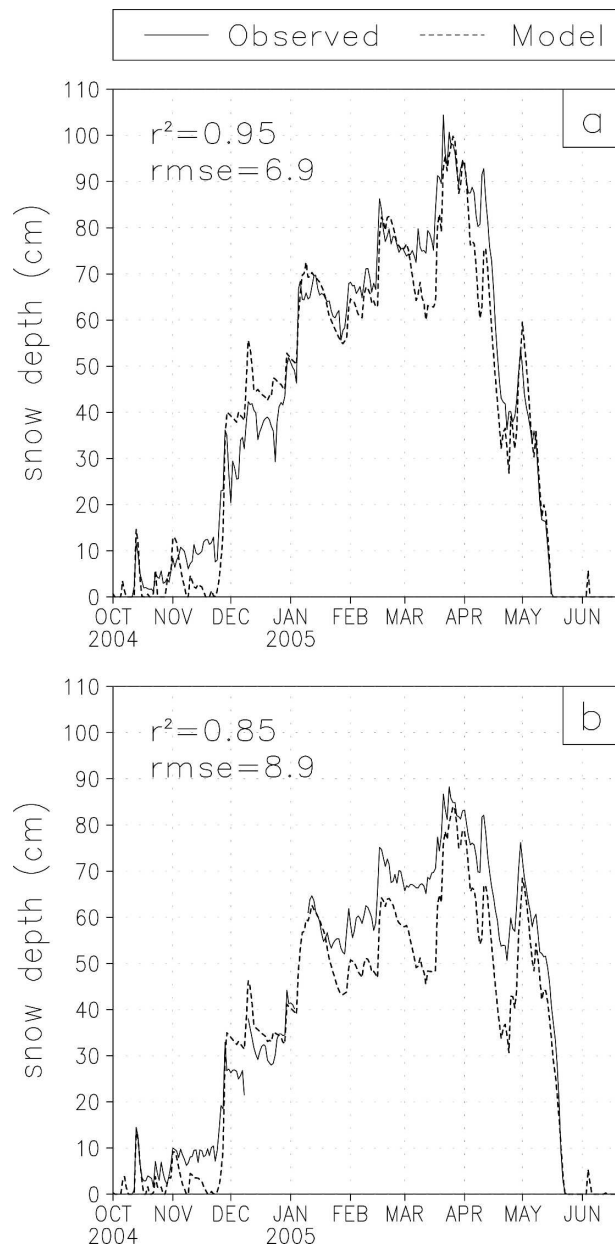


FIG. 8. Modeled snow depth evolution for the (a) clear-cut and (b) forested sites, and the observed depth evolution obtained from acoustic depth sensors.

were also performed for 1 October 2002 through 30 June 2003, and similar outcomes were produced (not shown). Further, the interannual variability was captured.

As a comparison of the model's combined spatial and temporal snow-evolution representation, simulations were performed over the USDA–Agricultural Research Service (USDA–ARS), Reynolds Mountain East (RME) watershed ( $0.38 \text{ km}^2$ ) in southwestern Idaho

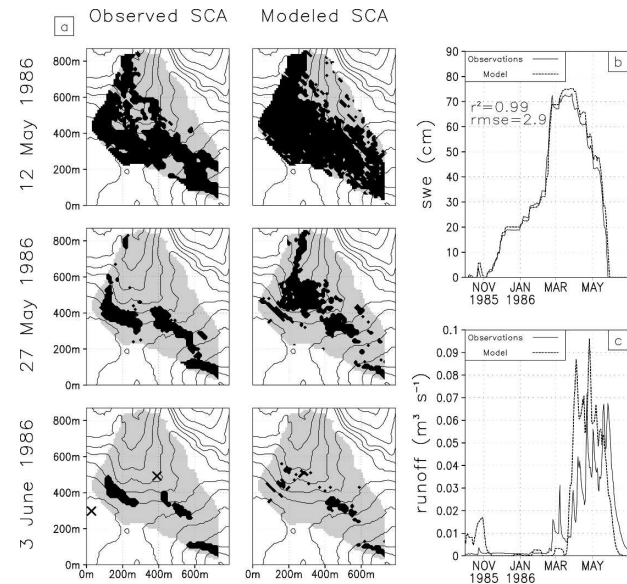


FIG. 9. Comparison of observed and modeled, 1 Oct 1985–30 Jun 1986, snow-related fields for the Reynolds Mountain East watershed: (a) snow-covered area during three 1986 snowmelt-period dates (black is the snow-covered area; gray is the observation mask), (b) snow pillow SWE, (c) stream discharge observations at the mouth of the basin compared with the basin-summed runoff simulated at the base of the snowpack; a 15-day running mean was applied to the modeled runoff to improve visibility. Locations of the hilltop and valley meteorological stations are identified by markers in the lower-left panel. The snow pillow is located near the valley meteorological station. The prevailing winter winds are from the southwest.

(Winstral and Marks 2002). Approximately 80% of the watershed vegetation is sagebrush, and the other 20% is a mix of conifer and aspen forest. The site includes two weather stations providing hourly data (air temperature, relative humidity, wind speed and direction, and undercatch-corrected precipitation) used in the simulations: a hilltop station located on the southwest border of the basin, and a forest-opening site located near the basin center (Fig. 9). The basin spans an elevation range of 2072 to 2137 m MSL, and the prevailing winter winds are from the southwest. Model simulations were performed during 1 October through 30 June, for 1985–86 and 1986–87, using 10-m horizontal grid increment. These two water years represent 128% and 66% of the average forest-opening site precipitation. See Winstral and Marks (2002) for additional information about the meteorological, topography, and vegetation datasets.

Figure 9a displays the observed and modeled snow-covered area during three 1986 snowmelt-period dates. These observations were obtained from a series of aerial photographs (Winstral and Marks 2002), and



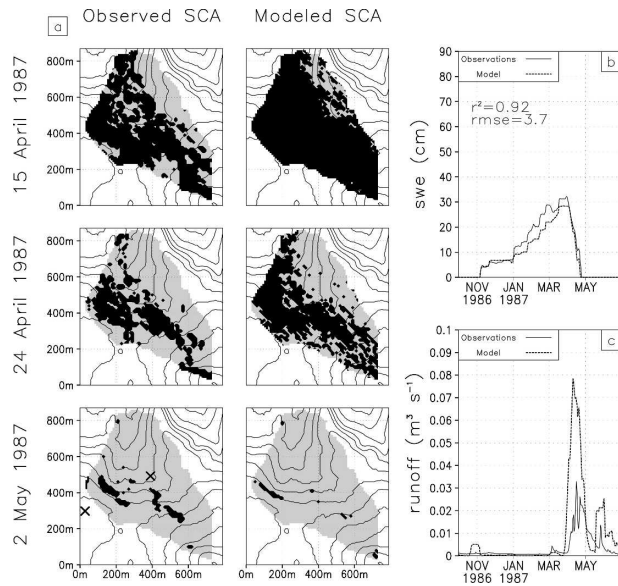


FIG. 10. Same as Fig. 9, except for 1986–87.

gridded to the model simulation grid. The relatively large modeled snow-cover distribution on 12 May, and the small distribution on 3 June, suggests the modeled snow-depth differences in the sheltered and unsheltered areas was underestimated; the thin-snow areas should have been thinner, and the deep-snow areas should have been deeper. Snow pillow SWE observations at the forest-clearing site compare favorably with the corresponding model grid cell (Fig. 9b). Stream discharge observations from a weir located at the mouth of the basin (Winstral and Marks 2002) are compared with the basin-summed runoff simulated at the base of the snowpack (Fig. 9c). While we recognize that these two quantities are not directly comparable due to early melt season contributions to soil moisture recharge and the time required for runoff routing from slopes to the gauge, the general timing and magnitudes should be similar and provide an integrated assessment of model behavior. The 1986–87 model simulation (Fig. 10) is similar to that of 1985–86, with the exception that this year had much less snow precipitation and there was a correspondingly shallower snowpack. As in the 1985–86 simulation, the model overestimated snow-covered area early in the melt period, suggesting that the snow redistribution model has not sufficiently eroded the snow in the observed snow-free areas, or that the model has not melted the shallow-snow areas quickly enough (Fig. 10a) due to, for example, protruding shrubs (Sturm et al. 2005a). SnowModel has captured the observed interannual variability (Figs. 9 and 10). Qualitatively, the SnowModel simulations are very similar to those simulated by Winstral and Marks (2002), even

though the two snow redistribution modeling approaches are quite different. Winstral and Marks (2002) define erosion and deposition sites according to the wind field at each time step, and SnowModel defines erosion and deposition sites according to blowing-snow transport equations (where the fluxes are wind field dependent). Because snow-transporting winds often come from a specific direction, Prasad et al. (2001) simulated snow distributions in an environment similar to that of Winstral and Marks (2002). They concluded the use of drift factors (defined to be propensity of a location to accumulate or erode snow), whose locations were identified prior to model simulations, also yielded acceptable snow distributions for many applications.

## 5. Discussion

### a. Applications

SnowModel was created to run on grid increments of 1 to 200 m and temporal increments of 10 min to 1 day. Using these spatial and temporal increments, the model can be configured to run for a year or more, simulating diurnal, synoptic, and seasonal cycles. Conceptually, SnowModel includes the first-order processes required to simulate snow evolution within each of the global snow classes [i.e., ice, tundra, taiga, alpine/mountain, prairie, maritime, and ephemeral defined by Sturm et al. (1995)]. Simulated processes include forest canopy interception, unloading, and sublimation (typical of taiga and alpine/mountain classes); blowing-snow redistribution and sublimation (typical of tundra, alpine/mountain, and prairie classes); and snow accumulation, snow-density evolution, and snowpack melt (typical of all snow classes).

Within the model, subgrid (spatial) processes are not accounted for; SnowModel assumes that each grid cell is horizontally homogeneous. This practice is typical of most snow and other hydrological modeling systems, and is appropriate depending on the scale of the processes of interest (Blöschl 1999). In forested landscapes, snow distribution mechanisms operate at scales of one to hundreds of meters, and fit within the typical 1–200-m SnowModel grid increments. In this environment, canopy-intercepted snow can lose mass by sublimation, and snow released from branches accumulates on the ground in nonuniform snow-depth patterns (Hedstrom and Pomeroy 1998; Pomeroy et al. 2002). At distances of tens to hundreds of meters, wind-blown snow is a dominant factor influencing the snow distribution in tundra, alpine/mountain, and prairie snow covers. This also fits within appropriate SnowModel grid-cell increments. In these environments, the fre-

quent occurrence of blowing snow leads to significant snow redistribution, causing it to accumulate in the lee of ridges, topographic depressions, and taller vegetation (e.g., Elder et al. 1991; Liston and Sturm 1998; Liston et al. 2002; Hiemstra et al. 2002). For conditions where it is important to account for subgrid snow variability, such as where model grid increments exceed the relevant process spatial scales (e.g., 500 m to 50 km), Liston (2004) provides a possible solution.

The SnowModel code includes an efficient parameter-definition and model-control component that makes simulations easily adaptable to new spatial and temporal domains and/or model configurations. For example, depending on application of interest, the following submodel combinations can be run: MicroMet (where, for example, only meteorological forcing is needed to drive another model); MicroMet and EnBal; MicroMet, EnBal, and SnowPack (where blowing snow is not of interest); MicroMet and SnowTran-3D (where melt is not of interest); or MicroMet, EnBal, SnowPack, and SnowTran-3D. The model can utilize a single meteorological station to thousands of stations, and it can account for a variety of vegetation and topographic configurations. In addition, a snow data assimilation module (Liston and Hiemstra 2006, manuscript submitted to *J. Hydrometeor.*) can be run with SnowModel to provide a simulated best fit to available snow observations. In addition to seasonal snow simulations, SnowModel has also recently been used to simulate winter and summer mass-balance evolution of the Mittivakkat Glacier in southeast Greenland (Mernild et al. 2006), and to analyze surface and subsurface melt patterns and quantities in Antarctica (Liston and Winther 2005). As an example of SnowModel computational constraints, full annual integrations using hourly time steps over domains as large as 50 km by 50 km with 30-m grid increments ( $\sim 3$  million grid cells) are achieved with readily available computational resources.

### b. Limitations

Over the years we have found SnowModel to be useful in a wide variety of applications. As part of its development we have also recognized limitations in our model formulation and identified numerous additions that could be made to the modeling system to enhance its general use. As an example, the figures presented herein suggest the model reproduces the basic observed patterns of subcanopy radiation, canopy-intercepted snow sublimation, snow depth and density evolution in forested and nonforested sites, and the observed snow distribution patterns in windy, temperate environ-

ments. But, a closer look at these outputs reveals model deficiencies.

As noted in the comparison of observed and modeled forest canopy-intercepted-snow sublimation rates, hourly simulated values were often either over- or underpredicted. When these values were summed, these errors generally canceled, producing a modeled mass balance that was comparable to the observed balance over the sublimation season (Fig. 2). Ideally, the model would accurately simulate the observed hourly values. Achieving this will require additional model development and testing. Other researchers have found similar discrepancies between observed and modeled canopy sublimation (e.g., Pomeroy et al. 1998b).

The daily averaged subcanopy incoming solar radiation was underpredicted during summer and overpredicted during spring and fall (Fig. 3). This may be related to a relationship between solar zenith angle and canopy structure, and might be accounted for by implementing a zenith angle dependence on  $k$  in Eq. (21). As noted by Sicart et al. (2004), the canopy extinction coefficient,  $\tau_v$ , is not very sensitive to effective leaf area index,  $LAI^*$ , and that  $k$  in Eq. (21) depends most strongly on the above-canopy radiation properties and the canopy structural characteristics. This suggests that  $k$  may also be forest-type dependent. In addition, the general model assumption of a uniform canopy does not allow it to account for radiation peaks that occur when the sun shines through open areas in the trees (Fig. 3b). The can partially be addressed by using the canopy gap-fraction parameter defined in Eq. (22). A summary of canopy radiation and associated microclimate issues can be found in Bonan (1991).

For simulation domains that span large elevation differences, air temperature and precipitation distributions simulated by MicroMet and used to drive SnowModel are strongly dependent upon the applied temperature lapse rates and precipitation scaling factors. These two parameters play important roles in defining both snow accumulation and ablation. Unfortunately, data required to accurately define these adjustment factors frequently do not exist. The problem is particularly acute when they vary spatially, such as in the case of local temperature inversions or orographic precipitation shadows. Results from future process-level studies can be incorporated in the model to improve these deficiencies.

The MicroMet approach to defining cloud-cover fraction by converting near-surface air temperature and relative humidity to temperature and humidity at 700 mb, and using this to calculate cloud fraction, does not always appear to be appropriate. For example, under

clear skies, nighttime radiational cooling can lead to high relative humidity near the surface while cloud cover remains a minimum. To improve this formulation, additional coincident surface and 700-mb meteorology and cloud fraction data are required.

There are also features in natural systems not considered in SnowModel. For example, the model assumes that vegetation cover in each model grid cell is uniform. Thus, the model is unable to appropriately simulate features like tree-wells (the depressions that form in the snow beneath individual tree canopies; Sturm 1992), nor is it able to simulate snow drifts that accumulate behind individual shrubs, such as occurs throughout shrublands of the western United States and Arctic (Sturm et al. 2005b). In addition, snow avalanches can play an important role in governing snow distributions in steep terrain (Elder et al. 1991; Blöschl and Kirnbauer 1992), and are also not currently represented within SnowModel.

To expand SnowModel's application, soil moisture and temperature submodels could also be included. This would extend the model's use to a wider range of ecological (e.g., Jones 1999; Sturm et al. 2005b) and hydrologic applications (e.g., Marsh 1999). To assist in validating model-generated runoff, SnowModel would benefit from the addition of a runoff routing scheme. A product of the SnowModel simulations is the computation of grid-cell snowmelt volumes during each model time step, and the associated grid-cell runoff. These outputs are available to drive soil moisture and runoff routing models, and would allow SnowModel to compare its hydrologic output to the river discharge hydrographs. This capability would provide a measure of model-simulated local to regional water balances over time scales ranging from individual storms and melt events to seasonal cycles.

## 6. Conclusions

SnowModel is a general purpose, spatially distributed, snow-evolution modeling system that includes a quasi-physically-based, high-resolution, meteorological distribution model (MicroMet). SnowModel is specifically designed to be applicable over a wide range of snow landscapes, climates, and conditions, including regions where blowing and drifting snow are important features of the environment. Since SnowModel's components were originally developed in nonforested environments where blowing snow is an important system component (e.g., arctic and alpine/mountain), here we have added routines to calculate sublimation of snow held within forest canopies and to modify incoming solar and longwave radiation for the presence

forests, and have compared the outputs with observations.

Snow covers throughout the world commonly exhibit important spatial (1–200 m) and temporal (diurnal) variability at the scales simulated by SnowModel. This variability is associated with differences in snow water equivalent and snow-covered area, and these differences, in turn, have important implications for the associated surface energy and moisture fluxes. As stated in the introduction, numerous studies have documented the impact these snow distributions have on energy transfers between the atmosphere, snow, and ground, and on the general climate system. Unfortunately, effective methods to scale up from finescale snow distributions to larger-scale climate systems are still in their infancy (e.g., Pomeroy et al. 1998a; Slater et al. 2001). SnowModel can simulate high-resolution snow properties and processes over a wide range of spatial domains, and could serve as a tool, for example, to help define subgrid snow distributions within the context of large-scale atmospheric and hydrologic models (Liston et al. 1999a; Luce et al. 1999; Liston 2004). In addition, it can be used to address sensitivities and vulnerabilities related to potential variations within earth's climate system. The model is also available to simulate snow-related processes in support of traditional hydrologic studies, and the ecological impacts of spatially and temporally varying snow distributions.

*Acknowledgments.* The authors thank Christopher A. Hiemstra for his work and comments regarding an early version of this model, including defining the SnowModel vegetation classification; Janet P. Hardy for providing the subcanopy longwave radiation observations; Adam Winstral and USDA-ARS Northwest Watershed Research Center for providing the Reynolds Mountain East datasets; Angus Goodbody for assisting with the Fraser Experimental Forest snow and meteorological data collection; and Christopher A. Hiemstra, Rudy King, John E. Strack, Ulrich Strasser, and two anonymous reviewers for their insightful reviews of this paper. This work was supported by NASA Grants NAG5-11710, NNG04GP59G, and NNG04HK191, NOAA Grant NA17RJ1228, and National Science Foundation Grant 0229973.

## REFERENCES

- Anderson, E. A., 1976: A point energy and mass balance model of a snow cover. NOAA Tech. Rep. NWS-19, 150 pp.
- Balk, B., and K. Elder, 2000: Combining binary decision tree and geostatistical methods to estimate snow distribution in a mountain watershed. *Water Resour. Res.*, **36**, 13–26.

- Barnes, S. L., 1964: A technique for maximizing details in numerical weather map analysis. *J. Appl. Meteor.*, **3**, 396–409.
- , 1973: Mesoscale objective analysis using weighted time-series observations. NOAA Tech. Memo. ERL NSSL-62, National Severe Storms Laboratory, Norman, OK, 60 pp.
- Bartelt, P., and M. Lehning, 2002: A physical SNOWPACK model for the Swiss avalanche warning. Part I: Numerical model. *Cold Reg. Sci. Technol.*, **35**, 123–145.
- Blöschl, G., 1999: Scaling issues in snow hydrology. *Hydrol. Processes*, **13**, 2149–2175.
- , and R. Kirnbauer, 1992: An analysis of snow cover patterns in a small Alpine catchment. *Hydrol. Processes*, **6**, 99–109.
- Bonan, G. B., 1991: A biophysical surface energy budget analysis of soil temperature in the boreal forests of interior Alaska. *Water Resour. Res.*, **27**, 767–781.
- Bruland, O., G. E. Liston, J. Vonk, and A. Killingtveit, 2004: Modelling the snow distribution at two High-Arctic sites at Svalbard, Norway, and at a Sub-Arctic site in Central Norway. *Nordic Hydrol.*, **35**, 191–208.
- Buck, A. L., 1981: New equations for computing vapor pressure and enhancement factor. *J. Appl. Meteor.*, **20**, 1527–1532.
- Chen, J. M., P. M. Rich, S. T. Gower, J. M. Norman, and S. Plummer, 1997: Leaf area index of boreal forests: Theory, techniques, and measurements. *J. Geophys. Res.*, **102**, 29 429–29 443.
- Cionco, R. M., 1978: Analysis of canopy index values for various canopy densities. *Bound.-Layer Meteor.*, **15**, 81–93.
- Cohen, J., and D. Entekhabi, 2001: The influence of snow cover on Northern Hemisphere climate variability. *Atmos.–Ocean*, **39**, 35–53.
- Dodson, R., and D. Marks, 1997: Daily air temperature interpolation at high spatial resolution over a large mountainous region. *Climate Res.*, **8**, 1–20.
- Elder, K., J. Dozier, and J. Michaelsen, 1991: Snow accumulation and distribution in an alpine watershed. *Water Resour. Res.*, **27**, 1541–1552.
- Ellis, A. W., and D. J. Leathers, 1999: Analysis of cold airmass temperature modification across the U.S. Great Plains as a consequence of snow depth and albedo. *J. Appl. Meteor.*, **38**, 696–711.
- Essery, R., and J. Pomeroy, 2004: Vegetation and topographic control of wind-blown snow distributions in distributed and aggregated simulations for an arctic tundra basin. *J. Hydrometeorol.*, **5**, 735–744.
- , —, J. Parviainen, and P. Storck, 2003: Sublimation of snow from coniferous forests in a climate model. *J. Climate*, **16**, 1855–1864.
- Fleagle, R. G., and J. A. Businger, 1980: *An Introduction to Atmospheric Physics*. Academic Press, 432 pp.
- Greene, E. M., G. E. Liston, and R. A. Pielke Sr., 1999: Simulation of above treeline snowdrift formation using a numerical snow-transport model. *Cold Reg. Sci. Technol.*, **30**, 135–144.
- Groisman, P. Ya., T. R. Karl, and T. W. Knight, 1994: Observed impact of snow cover on the heat balance and the rise of continental spring temperatures. *Science*, **263**, 198–200.
- Hardy, J., R. Melloh, G. Koenig, J. Pomeroy, A. Rowlands, D. Cline, K. Elder, and R. Davis, 2004a: Sub-canopy energetics at the CLPX Local Scale Observation Site (LSOS). National Snow and Ice Data Center, digital media.
- , —, —, D. Marks, A. Winstral, J. W. Pomeroy, and T. Link, 2004b: Solar radiation transmission through conifer canopies. *Agric. For. Meteorol.*, **126**, 257–270.
- Hasholt, B., G. E. Liston, and N. T. Knudsen, 2003: Snow distribution modelling in the Ammassalik Region, South East Greenland. *Nordic Hydrol.*, **34**, 1–16.
- Hedstrom, N. R., and J. W. Pomeroy, 1998: Measurements and modeling of snow interception in the boreal forest. *Hydrol. Processes*, **12**, 1611–1625.
- Hellström, R. Å., 2000: Forest cover algorithms for estimating meteorological forcing in a numerical snow model. *Hydrol. Processes*, **14**, 3239–3256.
- Hiemstra, C. A., G. E. Liston, and W. A. Reiners, 2002: Snow redistribution by wind and interactions with vegetation at upper treeline in the Medicine Bow Mountains, Wyoming, USA. *Arc. Antarct. Alp. Res.*, **34**, 262–273.
- Hinzman, L. D., D. L. Kane, C. S. Benson, and K. R. Everett, 1996: Energy balance and hydrological processes in an Arctic watershed. *Landscape Function: Implications for Ecosystem Response to Disturbance: A Case Study in Arctic Tundra*, J. F. Reynolds and J. D. Tenhunen, Eds., Ecologic Studies Series, Vol. 120, Springer-Verlag, 131–154.
- , D. J. Goering, and D. L. Kane, 1998: A distributed thermal model for calculating soil temperature profiles and depth of thaw in permafrost regions. *J. Geophys. Res.*, **103** (D22), 28 975–28 991.
- Iziomon, M. G., H. Mayer, and A. Matzarakis, 2003: Downward atmospheric longwave irradiance under clear and cloudy skies: Measurement and parameterization. *J. Atmos. Sol.-Terr. Phys.*, **65**, 1107–1116.
- Jones, H. G., 1999: The ecology of snow-covered systems: A brief overview of nutrient cycling and life in the cold. *Hydrol. Processes*, **13**, 2135–2147.
- Kane, D. L., L. D. Hinzman, C. S. Benson, and G. E. Liston, 1991: Snow hydrology of a headwater Arctic basin. 1. Physical measurements and process studies. *Water Resour. Res.*, **27**, 1099–1109.
- Koch, S. E., M. DesJardins, and P. J. Kocin, 1983: An interactive Barnes objective map analysis scheme for use with satellite and conventional data. *J. Climate Appl. Meteor.*, **22**, 1487–1503.
- Kunkel, K. E., 1989: Simple procedures for extrapolation of humidity variables in the mountainous western United States. *J. Climate*, **2**, 656–669.
- Lee, L. W., 1975: Sublimation of snow in a turbulent atmosphere. Ph.D. dissertation, University of Wyoming, 162 pp.
- Liston, G. E., 1995: Local advection of momentum, heat, and moisture during the melt of patchy snow covers. *J. Appl. Meteor.*, **34**, 1705–1715.
- , 2004: Representing subgrid snow cover heterogeneities in regional and global models. *J. Climate*, **17**, 1381–1397.
- , and D. K. Hall, 1995: An energy balance model of lake ice evolution. *J. Glaciol.*, **41**, 373–382.
- , and M. Sturm, 1998: A snow-transport model for complex terrain. *J. Glaciol.*, **44**, 498–516.
- , and R. A. Pielke Sr., 2001: A climate version of the regional atmospheric modeling system. *Theor. Appl. Climatol.*, **68**, 155–173.
- , and M. Sturm, 2002: Winter precipitation patterns in arctic Alaska determined from a blowing-snow model and snow-depth observations. *J. Hydrometeorol.*, **3**, 646–659.
- , and J.-G. Winther, 2005: Antarctic surface and subsurface snow and ice melt fluxes. *J. Climate*, **18**, 1469–1481.
- , and K. Elder, 2006: A meteorological distribution system for



- high resolution terrestrial modeling (MicroMet). *J. Hydrometeorol.*, **7**, 217–234.
- , R. A. Pielke Sr., and E. M. Greene, 1999a: Improving first-order snow-related deficiencies in a regional climate model. *J. Geophys. Res.*, **104** (D16), 19 559–19 567.
- , J.-G. Winther, O. Bruland, H. Elvehøy, and K. Sand, 1999b: Below-surface ice melt on the coastal Antarctic ice sheet. *J. Glaciol.*, **45**, 273–285.
- , —, —, —, —, and L. Karlöf, 2000: Snow and blue-ice distribution patterns on the coastal Antarctic ice sheet. *Antarct. Sci.*, **12**, 69–79.
- , J. P. McFadden, M. Sturm, and R. A. Pielke Sr., 2002: Modeled changes in arctic tundra snow, energy, and moisture fluxes due to increased shrubs. *Global Change Biol.*, **8**, 17–32.
- Luce, C. H., D. G. Tarboton, and K. R. Cooley, 1998: The influence of the spatial distribution of snow on basin-averaged snowmelt. *Hydrol. Processes*, **12**, 1671–1683.
- , —, and —, 1999: Sub-grid parameterization of snow distribution for an energy and mass balance snow cover model. *Hydrol. Processes*, **13**, 1921–1933.
- Marks, D., J. Domingo, D. Susong, T. Link, and D. Garen, 1999: A spatially distributed energy balance snowmelt model for application in mountain basins. *Hydrol. Processes*, **13**, 1935–1959.
- Marsh, P., 1999: Snowcover formation and melt: Recent advances and future prospects. *Hydrol. Processes*, **13**, 2117–2134.
- McFadden, J. P., G. E. Liston, M. Sturm, R. A. Pielke Sr., and F. S. Chapin III, 2001: Interactions of shrubs and snow in arctic tundra: Measurements and models. *Soil, Vegetation, Atmosphere Transfer Schemes and Large-Scale Hydrological Models*, A. J. Dolman et al., Eds., IAHS Publ. 270, 317–325.
- McNamara, J. P., D. L. Kane, and L. D. Hinzman, 1997: Hydrograph separations in an Arctic watershed using mixing model and graphical techniques. *Water Resour. Res.*, **33**, 1707–1719.
- , —, and —, 1999: An analysis an arctic channel network using a digital elevation model. *Geomorphology*, **29**, 339–353.
- Mernild, S. H., G. E. Liston, B. Hasholt, and N. T. Knudsen, 2006: Snow distribution and melt modeling for Mittivakkat Glacier, Ammassalik Island, southeast Greenland. *J. Hydrometeorol.*, **7**, 808–824.
- Montesi, J., K. Elder, R. A. Schmidt, and R. E. Davis, 2004: Sublimation of intercepted snow within a subalpine forest canopy at two elevations. *J. Hydrometeorol.*, **5**, 763–773.
- Nelson, F. E., K. M. Hinkel, N. I. Shiklomanov, G. R. Mueller, L. L. Miller, and D. K. Walker, 1998: Active-layer thickness in north central Alaska: Systematic sampling, scale, and spatial autocorrelation. *J. Geophys. Res.*, **103** (D22), 28 963–28 973.
- Pomeroy, J. W., and R. A. Schmidt, 1993: The use of fractal geometry in modeling intercepted snow accumulation and sublimation. *Proc. 50th Eastern Snow Conf.*, Quebec City, QC, Canada, Eastern Snow Conference, 1–10.
- , D. M. Gray, K. R. Shook, B. Toth, R. L. H. Essery, A. Pietroniro, and N. Hedstrom, 1998a: An evaluation of snow accumulation and ablation processes for land surface modeling. *Hydrol. Processes*, **12**, 2339–2367.
- , J. Parviainen, N. Hedstrom, and D. M. Gray, 1998b: Coupled modeling of forest snow interception and sublimation. *Hydrol. Processes*, **12**, 2317–2337.
- , D. M. Gray, N. R. Hedstrom, and J. R. Janowics, 2002: Prediction of seasonal snow accumulation in cold climate forests. *Hydrol. Processes*, **16**, 3543–3558.
- Prasad, R., D. G. Tarboton, G. E. Liston, C. H. Luce, and M. S. Seyfried, 2001: Testing a blowing snow model against distributed snow measurements at Upper Sheep Creek, Idaho, USA. *Water Resour. Res.*, **37**, 1341–1357.
- Ryan, B. C., 1977: A mathematical model for diagnosis and prediction of surface winds in mountainous terrain. *J. Appl. Meteorol.*, **16**, 571–584.
- Schmidt, R. A., 1972: Sublimation of wind-transported snow—A model. Research Paper RM-90, Rocky Mountain Forest and Range Experiment Station, Forest Service, U.S. Department of Agriculture, Fort Collins, CO, 24 pp.
- Sicart, J. E., J. W. Pomeroy, R. L. H. Essery, J. Hardy, T. Link, and D. Marks, 2004: A sensitivity study of daytime net radiation during snowmelt to forest canopy and atmospheric conditions. *J. Hydrometeorol.*, **5**, 774–784.
- Slater, A. G., and Coauthors, 2001: The representation of snow in land surface schemes: Results from PILPS 2(d). *J. Hydrometeorol.*, **2**, 7–25.
- Strack, J. E., R. A. Pielke Sr., and J. Adegoke, 2003: Sensitivity of model-generated daytime surface heat fluxes over snow to land-cover changes. *J. Hydrometeorol.*, **4**, 24–42.
- Sturm, M., 1992: Snow distribution and heat flow in the taiga. *Arc. Alp. Res.*, **24**, 145–152.
- , J. Holmgren, and G. E. Liston, 1995: A seasonal snow cover classification system for local to global applications. *J. Climate*, **8**, 1261–1283.
- , J. P. McFadden, G. E. Liston, F. S. Chapin III, C. H. Racine, and J. Holmgren, 2001: Snow–shrub interactions in arctic tundra: A hypothesis with climatic implications. *J. Climate*, **14**, 336–344.
- , T. Douglas, C. Racine, and G. E. Liston, 2005a: Changing snow and shrub conditions affect albedo with global implications. *J. Geophys. Res.*, **110**, G01004, doi:10.1029/2005JG000013.
- , J. Schimel, G. Michelson, J. Welker, S. F. Oberbauer, G. E. Liston, J. Fahnestock, and V. E. Romanovsky, 2005b: Winter biological processes could help convert arctic tundra to shrubland. *Bioscience*, **55**, 17–26.
- Taras, B., M. Sturm, and G. E. Liston, 2002: Snow–ground interface temperatures in the Kuparuk River Basin, arctic Alaska: Measurements and model. *J. Hydrometeorol.*, **3**, 377–394.
- Tarboton, D. G., T. G. Chowdhury, and T. H. Jackson, 1995: A spatially distributed energy balance snowmelt model. *Biogeochemistry of Seasonally Snow-Covered Catchments*, K. A. Tonnessen, M. W. Williams, and M. Tranter, Eds., IAHS Publ. 228, 141–155.
- Thornton, P. E., S. W. Running, and M. A. White, 1997: Generating surfaces of daily meteorological variables over large regions of complex terrain. *J. Hydrol.*, **190**, 214–251.
- Thorpe, A. D., and B. J. Mason, 1966: The evaporation of ice spheres and ice crystals. *Brit. J. Appl. Phys.*, **17**, 541–548.
- Troendle, C. A., and J. O. Reuss, 1997: Effect of clear cutting on snow accumulation and water outflow at Fraser, Colorado. *Hydrol. Earth Syst. Sci.*, **1**, 325–332.
- Tucker, C., D. Slayback, J. Pinzon, S. Los, R. Myneni, and M. Taylor, 2001: Higher northern latitude NDVI and growing season trends from 1982 to 1999. *Int. J. Biometeorol.*, **45**, 184–190.
- Wahl, K. L., 1992: Evaluation of trends in runoff in the western United States. *Managing Water Resources during Global*

- Change, R. Herrmann, Ed., American Water Resources Association, 701–710.
- Walcek, C. J., 1994: Cloud cover and its relationship to relative humidity during a spring midlatitude cyclone. *Mon. Wea. Rev.*, **122**, 1021–1035.
- Wallace, J. M., and P. V. Hobbs, 1977: *Atmospheric Science: An Introductory Survey*. Academic Press, 467 pp.
- Winstral, A., and D. Marks, 2002: Simulating wind fields and snow redistribution using terrain-based parameters to model snow accumulation and melt over a semi-arid mountain catchment. *Hydrol. Processes*, **16**, 3585–3603.
- , K. Elder, and R. E. Davis, 2002: Spatial snow modeling of wind-redistributed snow using terrain-based parameters. *J. Hydrometeor.*, **3**, 524–538.
- Zhang, T., R. L. Armstrong, and J. Smith, 2003: Investigation of the near-surface soil freeze-thaw cycle in the contiguous United States: Algorithm development and validation. *J. Geophys. Res.*, **108** (D22), 8860, doi:10.1029/2003JD003530.